Mon. Not. R. Astron. Soc. **325,** 483–496 (2001)

The 2dF QSO Redshift Survey – II. Structure and evolution at high redshift

Scott M. Croom,[1,2★] T. Shanks,[3] B. J. Boyle,[2] R. J. Smith,[4] L. Miller,[5] N. S. Loaring[5] and F. Hoyle[3]

[1]*Imperial College of Science, Technology and Medicine, Blackett Laboratory, Prince Consort Road, London SW7 2BW*
[2]*Anglo-Australian Observatory, PO Box 296, Epping, NSW 2121, Australia*
[3]*Physics Department, University of Durham, South Road, Durham DH1 3LE*
[4]*Research School of Astronomy and Astrophysics, ANU, Private Bag, Weston Creek PO, ACT 2611, Australia*
[5]*Department of Physics, Oxford University, Keble Road, Oxford OX1 3RH*

Accepted 2001 February 2. Received 2001 February 2; in original form 2000 September 18

ABSTRACT

In this paper we present a clustering analysis of QSOs over the redshift range $z = 0.3$–2.9. We use a sample of 10 558 QSOs taken from the preliminary data release catalogue of the 2dF QSO Redshift Survey (2QZ). The two-point redshift-space correlation function of QSOs, $\xi_{\rm Q}(s)$, is shown to follow a power law on scales $s \simeq 1$–$35\,h^{-1}$ Mpc. Fitting a power law of the form $\xi_{\rm Q}(s) = (s/s_0)^{-\gamma}$ to the QSO clustering averaged over the redshift interval $0.3 < z \leq 2.9$, we find $s_0 = 3.99^{+0.28}_{-0.34}\,h^{-1}$ Mpc and $\gamma = 1.58^{+0.10}_{-0.09}$ for an Einstein–de Sitter cosmology. The effect of a significant cosmological constant, λ_0, is to increase the separation of QSOs, so that with $\Omega_0 = 0.3$, $\lambda_0 = 0.7$ the power law extends to $\simeq 60\,h^{-1}$ Mpc and the best fit is $s_0 = 5.69^{+0.42}_{-0.50}\,h^{-1}$ Mpc and $\gamma = 1.56^{+0.10}_{-0.09}$. These values, measured at a mean redshift of $\bar{z} = 1.49$, are comparable to the clustering of local optically selected galaxies. We compare the clustering of 2QZ QSOs with generic cold dark matter (CDM) models with shape parameter $\Gamma_{\rm eff}$. Standard CDM with $\Gamma_{\rm eff} = 0.5$ is ruled out in both Einstein–de Sitter and cosmological constant dominated cosmologies, where $\Gamma_{\rm eff} \simeq 0.2$–$0.4$ and $\Gamma_{\rm eff} \simeq 0.1$–$0.2$ respectively are the allowable ranges.

We measure the evolution of QSO clustering as a function of redshift. For $\Omega_0 = 1$ and $\lambda_0 = 0$ there is no significant evolution in comoving coordinates over the redshift range of the 2QZ. QSOs thus have similar clustering properties to local galaxies at all redshifts that we sample. In the case of $\Omega_0 = 0.3$ and $\lambda_0 = 0.7$, QSO clustering shows a marginal increase at high redshift, s_0 being a factor of $\sim$1.4 higher at $z \simeq 2.4$ than at $z \simeq 0.7$. Although the clustering of QSOs is measured on large scales where linear theory should apply, the evolution of QSO clustering does not follow the linear theory predictions for growth via gravitational instability (rejected at the $>$99 per cent confidence level). A redshift-dependent bias is required to reconcile QSO clustering observations with theory. A simple biasing model, in which QSOs have cosmologically long lifetimes (or alternatively form in peaks above a constant threshold in the density field), is acceptable in an $\Omega_0 = 1$ cosmology, but is only marginally acceptable if $\Omega_0 = 0.3$ and $\lambda_0 = 0.7$. Biasing models in which QSOs are assumed to form over a range in redshift, based on the Press–Schechter formalism, are consistent with QSO clustering evolution for a minimum halo mass of $\sim 10^{12}$ and $\sim 10^{13}\,{\rm M}_{\odot}$ in an Einstein–de Sitter and cosmological constant dominated universe, respectively. However, until an accurate, physically motivated model of QSO formation and evolution is developed, we should be cautious in interpreting the fits to these biasing models.

Key words: galaxies: clusters: general – quasars: general – cosmology: observations – large-scale structure of Universe.

★E-mail: scroom@aaoepp.aao.gov.au

© 2001 RAS

1 INTRODUCTION

The 2dF QSO Redshift Survey (2QZ) aims to compile a homogeneous catalogue of ∼25 000 QSOs using the Anglo-Australian Telescope (AAT) 2-degree Field facility (2dF: Taylor, Cannon & Watson 1997). This catalogue will constitute a factor of ≳50 increase in numbers to a equivalent flux limit over previous data sets (e.g. Boyle et al. 1990). The main science goal of the 2QZ is to use QSOs to probe the large-scale structure of the Universe over a range of scales from 1 to $1000\,h^{-1}$ Mpc, and in the redshift interval $0.3 \lesssim z \lesssim 2.9$.

Clustering of QSOs at small to intermediate scales (1–$50h^{-1}$ Mpc) supplies a wealth of information on large-scale structure. QSOs still give us the only method of directly determining the three-dimensional clustering of high-redshift objects within a large enough volume for it to be truly representative. When complete, the 2QZ will sample a volume of $1.5 \times 10^9\,h^{-3}$ Mpc^3 (for $\Omega_0 = 1$), an order of magnitude larger than current galaxy redshift surveys (e.g. the 2dF Galaxy Redshift Survey: Colless 1999). This large volume also allows us to probe the scales where linear evolution occurs, simplifying comparisons with theory.

The shape and amplitude of the two-point autocorrelation function, $\xi(r)$, are determined by two factors. The first is the distribution of matter fluctuations in the Universe. This depends on fundamental physics, such as the growth of structure via gravitational instability and the initial spectrum of fluctuations. The second factor concerns the complex and generally non-linear physics which occurs during galaxy and QSO formation. The difference between the matter and galaxy or QSO distributions is commonly called bias, $b(r, z)$, such that

$$\xi_{\rm Q}(r, z) = b^2(r, z)\xi_\rho(r, z), \tag{1}$$

where $\xi_{\rm Q}(r, z)$ and $\xi_\rho(r, z)$ are the two-point correlation functions of QSOs and the density field respectively. Both are functions of scale, r, and redshift, z. Often, a linear bias is assumed, which has no scale dependence, and it appears likely that for any local process of galaxy formation b should tend to a constant value on scales where the density perturbations are linear (e.g. Peacock 1997; Mann, Peacock & Heavens 1998). We will assume a linear bias throughout this paper.

The first attempt to measure the clustering of QSOs was made by Osmer (1981). Shaver (1984) was the first to detect QSO clustering on small scales, although in an inhomogeneous sample. Shanks et al. (1987) made the first detection of clustering at $\lesssim 10\,h^{-1}$ Mpc in a complete and uniformly selected sample, part of the Durham/AAT survey (Boyle et al. 1990). A number of authors have used this and other QSO samples to measure clustering. They all reach generally the same conclusions that clustering is detected at the ∼3σ–4σ level and is approximately consistent with a clustering scalelength $r_0 \sim 6h^{-1}$ Mpc, similar to local galaxy clustering, at a mean redshift of $z \sim 1.4$ (Iovino & Shaver 1988; Andreani & Cristiani 1992; Mo & Fang 1993; Shanks & Boyle 1994; Croom & Shanks 1996, hereafter CS96). There has been significant disagreement over the redshift evolution of QSO clustering, including claims for a decrease in the QSO correlation length (r_0) with redshift (Iovino & Shaver 1988), an increase in r_0 with redshift (La Franca, Andreani & Cristiani 1998, hereafter LAC98) and no change with redshift (CS96).

The measurement of galaxy clustering at high redshift has also taken dramatic steps forward in recent years. A number of surveys have made measurements of the clustering strength of galaxies up to $z \sim 1$. These samples typically contain a few hundred to a thousand galaxies over relatively small areas. The Canada–France Redshift Survey (CFRS) shows a significant decrease in clustering amplitude on scales $<2\,h^{-1}$ Mpc (Le Fevre et al. 1996). However, larger samples, such as the Canadian Network for Observational Cosmology-2 (CNOC-2) survey (Carlberg et al. 1999), show much slower evolution, with a gradual decrease of clustering with redshift: $r_0(z) \propto (1 + z)^{-0.3\pm0.2}$. Deep wide-field (∼ few degrees) imaging surveys used to measure the angular correlation function of galaxies also suggest higher clustering amplitudes than found in the CFRS (Postman et al. 1998). The differences found between these samples are partly due to the different selection methods (e.g. magnitude limits, photometric bands) used. It is likely that different galaxy types cluster differently, e.g. optically versus infrared selected galaxies (Peacock 1997). Clustering is also likely to be a function of galaxy luminosity. It is possible that this is the case for QSOs, although we leave the discussion of luminosity-dependent clustering of QSOs to a future paper. We note, however, that because of the stong luminosity evolution of QSOs (e.g. Boyle et al. 2000), an apparent magnitude limited survey of QSOs samples approximately the same part of the luminosity function at all redshifts up to $z \sim 2$. A second effect responsible for the difference in galaxy clustering results is cosmic variance arising from the small volumes and scales sampled, in particular by the CFRS. A key element of the 2QZ is that it is large enough to minimize any effects of cosmic variance on scales smaller than a few hundred h^{-1} Mpc. Although studies of galaxy clustering have been typically limited to $z \lesssim 1$, Steidel et al. (1998) have used galaxies detected by their Lyman break to derive the clustering properties of galaxies at $z \sim 3$. These observations show that the clustering of $L \sim L^*$ galaxies at $z \sim 3$ is also similar to that of local galaxies on scales $\lesssim 10\,h^{-1}$ Mpc, with $r_0 \simeq 4$–$6h^{-1}$ Mpc depending on the assumed cosmology (Adelberger et al. 1998).

In this paper we look at QSO clustering in the 2QZ on scales from ∼1 to $100\,h^{-1}$ Mpc. We do not attempt to study larger scales because of the current non-uniformity of the data set. This will be reserved for future work, on completion of the survey. In Section 2 we describe the 2QZ data used and our methods of analysis. In Sections 3 and 4 we present our clustering results, and compare them with physical models. Our conclusions are presented in Section 5.

2 DATA AND TECHNIQUES

2.1 The 2dF QSO redshift survey

For the analysis in this paper we have used the first public release catalogue of the 2QZ containing 10 681 QSOs (the 10k catalogue). This 10k catalogue contains the most spectroscopically complete fields observed prior to 2000 November, and will be released to the astronomical community in the first half of 2001 (Croom et al. 2001). The sample contains 10 558 QSOs in the redshift range $0.3 < z \leq 2.9$ which will be included in our analysis below.

The identification of QSO candidates for the 2QZ was based on broad-band ub_Jr colours from Automatic Plate Measuring (APM) facility measurements of UK Schmidt Telescope (UKST) photographic plates. The survey comprises 30 UKST fields, arranged in two $75^\circ \times 5^\circ$ declination strips centred in the South Galactic Cap (SGC) at $\delta = -30^\circ$ and the North Galactic Cap (NGC) at $\delta = 0^\circ$ with RA ranges $\alpha = 21^{\rm h}40$ to $3^{\rm h}15$ and $9^{\rm h}50$ to $14^{\rm h}50$ respectively. Each UKST field contains independent CCD calibration (Boyle, Shanks & Croom 1995; Croom et al. 1999). The completed survey will cover approximately 740 deg^2 (some areas

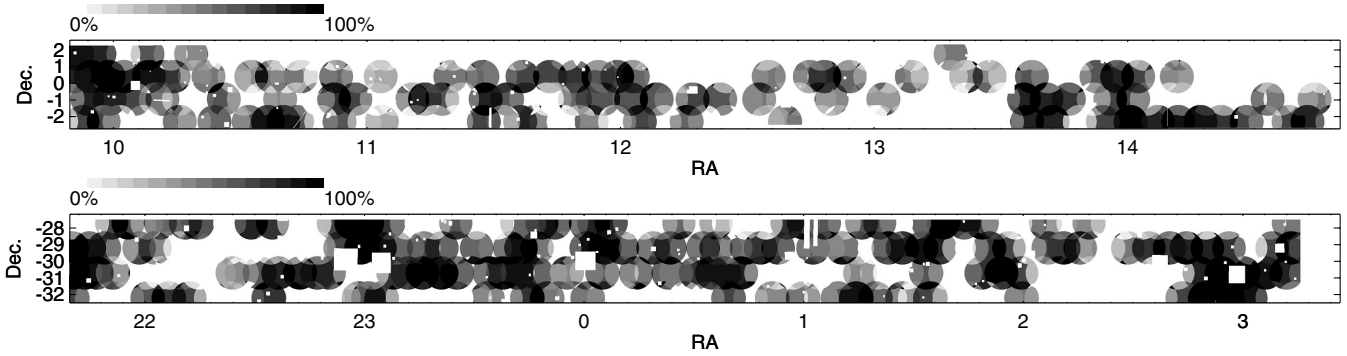

Figure 1. The current fractional coverage in the NGC (top) and SGC (bottom) strips of the 2QZ. Each circular region corresponds to one 2dF pointing. The coverage is the fraction of QSO candidates observed in each region. The small rectangular holes correspond to regions containing bright stars and plate defects.

having been removed because of bright stars, plate defects etc). Further details of the photometric catalogue can be found in Croom (1997), Smith (1998) and Smith et al. (2001).

Spectroscopic observations have been carried out using the 2dF instrument at the AAT in conjunction with the 2dF Galaxy Redshift Survey (Colless et al. 1999), as the 2QZ and galaxy survey areas cover the same regions of sky. Typically, 225 fibres are devoted to galaxies, 125 to QSO candidates and 25–30 to sky in each 2dF observation. Spectroscopic data are reduced using the 2dF pipeline reduction system (Bailey & Glazebrook 1999). The identification of QSO spectra and redshift estimation was carried out using the AUTOZ code written specifically for this project (Miller et al., in preparation). This program compares template spectra of QSOs, stars and galaxies with the observed spectra. Identifications are then confirmed by eye for all spectra. Spectroscopic completeness is typically >80 per cent when observations are made in reasonable or good conditions. In the analysis below we use all objects that have been classified as class 1 QSOs (class 1 being the highest quality identification; objects classified as class 2 IDs or 'QSO?' were not included) and which were observed in fields within the 10k catalogue (which is limited to ≥85 per cent spectroscopic completeness).

2.2 Correlation function estimates

As the QSO correlation function, $\xi_{\rm Q}$, probes high redshifts and large scales, the measured values are highly dependent on the assumed cosmology. We employ the method of Osmer (1981), which uses the coordinate transform in the Robertson–Walker metric (Weinberg 1972) to determine the comoving separation of pairs of QSOs. We choose to calculate $\xi_{\rm Q}$ for two representative cosmological models: $(\Omega_0, \lambda_0) = (1, 0)$ and $(0.3, 0.7)$, where Ω_0 and λ_0 represent the conventional mass and vacuum energy (cosmological constant) density contribution, respectively, to the total energy density of the Universe. We will call these cosmological models EdS (Einstein–de Sitter) and Λ respectively.

We have used the minimum variance estimator suggested by Landy & Szalay (1993) to calculate $\xi(s)$, where s is the redshift-space separation of two QSOs. This estimator is

$$\xi_{\rm Q}(s) = \frac{QQ(s) - 2QR(s) + RR(s)}{RR(s)}, \qquad (2)$$

where QQ, QR and RR are the number of QSO–QSO, QSO–random and random–random pairs counted at separation $s \pm \Delta s/2$. We bin our pairs such that $\log(\Delta s) = 0.1$ or 0.2. The density of random points used is 50 times the density of QSOs.

The area of the survey is covered by a mosaic of 2dF pointings.

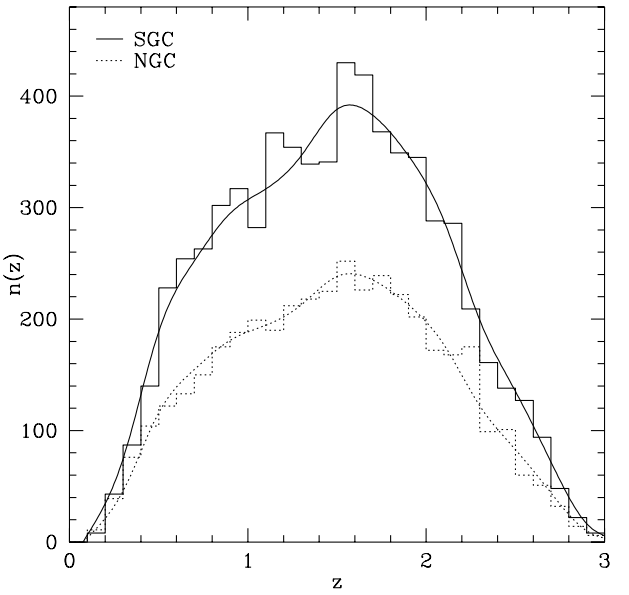

Figure 2. The redshift distribution of QSOs in the 10k catalogue for the NGC (dotted histogram) and SGC (solid histogram) strips. Also shown is the fit used to generate random redshift distributions (smooth curves), normalized to the number of QSOs in each slice.

These pointings overlap in order to obtain complete coverage in all areas, including regions of high galaxy and QSO density. As the survey is not yet complete, this means that certain areas within 2dF fields will not have had all candidates observed, and therefore the observational completeness of the sample varies strongly with angular position on the sky. This variation in observational completeness can clearly be seen in Fig. 1. Where a large number of 2dF pointings overlap the coverage is ∼100 per cent, while in overlap regions that have yet to be observed a second or third time the completeness is significantly lower. Particular care has been taken to construct the random point distribution so as to take into account this angular selection function. In each region defined by the intersection of 2dF fields, we have counted the number of QSO candidates observed and compared this with the total number to calculate the fractional observational completeness. We then weight the probability of a random being placed in that region by this fractional completeness. This corrects for the angular incompleteness arising from overlapping 2dF fields.

Our candidate density is not completely uniform over the length of the strips, owing to an increase in stellar contamination in areas closer to the Galactic plane. In addition, small residual calibration

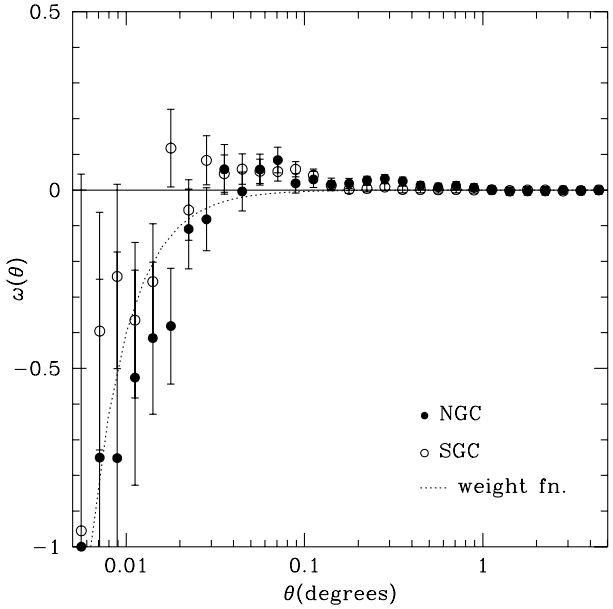

Figure 3. The angular correlation function for all currently observed candidates in the 2QZ, split into the NGC (filled circles) and SGC (open circles). A deficit of pairs on small scales owing to 2dF positioning constraints can be seen. The dotted line denotes the weight function used to correct for the lack of close pairs. The uniformity at large scales, $>0.^{\circ}1$, demonstrates the effectiveness of our correction for the non-uniform field coverage.

errors in the relative magnitude zero-points of the UKST plates could add spurious structure on large scales. Any possible offsets are being corrected by calibration from further CCD photometry; however, in this paper we will correct for this effect by normalizing the number of random points to the number of QSOs with spectroscopically determined redshifts in each UKST field. This correction will clearly remove power on large scales, which is why we do not discuss structure on scales larger than $\sim 100\,h^{-1}$ Mpc in this paper. After constructing the angular mask, we then assign the random points a random redshift, taken from a spline fit to the binned ($\Delta z = 0.2$) redshift distribution of the full 2QZ sample (changing Δz by a factor of 2 makes no observable difference to $\xi_{\rm Q}$). The redshift distributions for the NGC and SGC data sets are shown in Fig. 2. The fit used to generate the redshift distribution for the random points is also shown (the smooth curves in Fig. 2), in each case normalized to the number of QSOs in each 2QZ strip. The above process for correcting observational completeness and calculating $\xi_{\rm Q}$ we call method 1.

We have tested the effectiveness of this process by making comparisons with correlation functions derived using two other methods. The first (method 2) is to calculate the correlation function from regions of the survey that have no overlapping fields still to be observed, that is, they have $\sim$100 per cent observational coverage. The number of QSOs in these regions is significantly less that in the total sample, reducing the signal-to-noise ratio in $\xi_{\rm Q}$. The second comparison method (method 3) is to allocate each random point an (α, δ) taken from the QSO catalogue, so that the random distribution has *exactly* the same angular distribution as the QSOs. The redshifts of the random points are then allocated using the spline fit discussed above.

Two other observational biases could, in principle, affect our measurements of $\xi_{\rm Q}$. The first is due to the fact that the 2dF instrument cannot position two fibres closer than $\sim$30 arcsec. We are therefore currently biased against QSO pairs with small angular separation (this problem is being remedied by independent follow-up of close QSO pairs). We have measured the angular correlation function of observed candidates, which shows this bias (see Fig. 3). Measuring the extent of the anticorrelation in Fig. 3 allows us to correct for the close pairs bias. The dotted line, which traces the anticorrelation, is $\omega(\theta) = 4.0 \times 10^{-5}\theta^{-2}$, and this can be used to construct a function

$$W_{\rm cp}(\theta) = \frac{1}{1 - 4.0 \times 10^{-5}\theta^{-2}}, \tag{3}$$

which is the weight function for close pairs separated by θ degrees. In practice this correction makes no difference to the measured correlation function, as almost all of the QSO pairs with small angular separations have widely differing redshifts, and the weighting of a small number of pairs has a negligible effect on large scales.

Extinction by Galactic dust will also imprint a signal on the angular distribution of the QSOs. Primarily this changes the effective magnitude limit in $b_{\rm J}$ by $A_{b_{\rm J}} = 4.035 \times E(B-V)$, where we use the dust reddening $E(B-V)$ as a function of position calculated by Schlegel, Finkbeiner & Davis (1998). We then weight the random distribution according to the reduction in number density caused by the extinction, such that

$$W_{\rm ext}(\alpha, \delta) = 10^{-\beta A_{b_{\rm J}}(\alpha,\delta)}, \tag{4}$$

where β is the slope of the QSO number counts at the magnitude limit of the survey. At $b_{\rm J} = 20.85$, the magnitude limit of the 2QZ, the QSO number counts are flat, with $\beta \simeq 0.3$. Again we find that applying this correction makes no significant difference to the measured $\xi_{\rm Q}$.

It can be useful to present clustering results in a non-parametric form, specified by the clustering amplitude within a given comoving radius, rather than as a scalelength that depends on a power-law fit to $\xi_{\rm Q}$. This is generally represented by the integrated correlation function, $\bar{\xi}$, within a given radius in redshift space, $s_{\rm max}$:

$$\bar{\xi}(s_{\rm max}) = \frac{3}{s_{\rm max}^3}\int_0^{s_{\rm max}} \xi(x) x^2\,{\rm d}x. \tag{5}$$

Authors tend to choose a variety of values for $s_{\rm max}$, e.g. $s_{\rm max} = 10h^{-1}$ Mpc (Shanks & Boyle 1994; Croom & Shanks 1996) or $s_{\rm max} = 15h^{-1}$ Mpc (LAC98). The choice is a compromise, selecting the scale for which a significant signal is seen. It is easiest to relate these measurements to theory for large scales, where linear evolution occurs. Below we will quote clustering amplitudes with $s_{\rm max} = 20h^{-1}$ Mpc, as this is a scale at which evolution should be linear to better than a few per cent. We note that choosing a large radius also reduces the effects of small-scale peculiar velocities and redshift measurement errors, which may well be a function of redshift.

We calculate the errors on $\xi_{\rm Q}$ using the Poisson estimate of

$$\Delta\xi(s) = \frac{1 + \xi(s)}{\sqrt{QQ(s)}}. \tag{6}$$

At small scales, $\lesssim 50\,h^{-1}$ Mpc, this estimate is accurate because each QSO pair is independent (i.e. the QSOs are not generally part of another pair at scales smaller than this). On larger scales the QSOs pairs become more correlated and we use the approximation that $\Delta\xi(s) = [1 + \xi(s)]/\sqrt{N_{\rm Q}}$, where $N_{\rm Q}$ is the total number of QSOs used in the analysis (Shanks & Boyle 1994; CS96). In this paper, we will generally be concerned with analysis on small scales ($\lesssim 50\,h^{-1}$ Mpc), where the Poisson error estimates are applicable. As a confirmation of our Poisson error estimates we have also derived field-to-field errors, by splitting the NGC and SGC strips

into two, and determining the scatter between the resulting four independent regions. The errors determined in this fashion are approximately equal to or less than the Poisson errors. We also test bootstrap errors which are found to be $\sim\sqrt{3}$ times greater than Poisson on all scales of interest, in agreement with expected theory (Mo, Jing & Borner 1992) and previous measurements (e.g. Shanks & Boyle 1994; CS96). On small scales, $\lesssim 2\,h^{-1}$ Mpc, the number of QSO–QSO pairs can be $\lesssim 10$. In this case simple root-n errors (equation 6) do not give the correct upper and lower confidence limits for a Poisson distribution. We use the formulae of Gehrels (1986) to estimate the Poisson confidence intervals for one-sided 84 per cent upper and lower bounds (corresponding to 1σ for Gaussian statistics). These errors are applied to our data for $QQ(s) < 20$. By this point, root-n errors adequately describe the Poisson distribution.

2.3 Fitting models to $\xi(s)$

Below we make comparisons of the data with a number of models, both simple functional forms (power laws) and more complex, physically motivated models [e.g. cold dark matter (CDM)]. We use the maximum likelihood method to determine the best-fitting parameters. The likelihood estimator is based on the Poisson probability distribution function, so that

$$L = \prod_{i=1}^{N} \frac{\mathrm{e}^{-\mu}\mu^{\nu}}{\nu} \tag{7}$$

is the likelihood, where ν is the observed number of QSO–QSO pairs, μ is the expectation value for a given model, and N is the number of bins fitted. We fit the data with bins $\Delta\log r = 0.1$, although we note that varying the bin size by a factor of 2 makes no noticeable difference to the resultant fit. In practice we minimize the function $S = -2\ln L$, and determine the errors from the distribution of ΔS, where ΔS is assumed to be distributed as χ^2. This procedure does not give us an absolute measurement of the goodness-of-fit for a particular model. We therefore also derive a value of χ^2 for each model fit in order to confirm that it is a reasonable description of the data. In particular this is appropriate when fitting on moderate to large scales ($\gtrsim 5\,h^{-1}$ Mpc), where the pair counts are large enough that the Poisson errors are well described by Gaussian statistics.

3 THE CORRELATION FUNCTION OF 2QZ QSOs

Here we present the results of our clustering analysis on an initial sample of 2QZ QSOs. This sample contains 10 558 QSOs taken from the 2QZ 10 k catalogue. Fig. 4 shows the distribution of QSOs projected on to a plane of constant declination. We note that the current distribution is highly non-uniform, as the survey is only partially complete.

3.1 The redshift-averaged QSO correlation function

We first measure the QSO two-point correlation function averaged over the entire redshift interval $0.3 < z \leq 2.9$. For an EdS cosmology we estimate ξ_{Q} using the three different processes

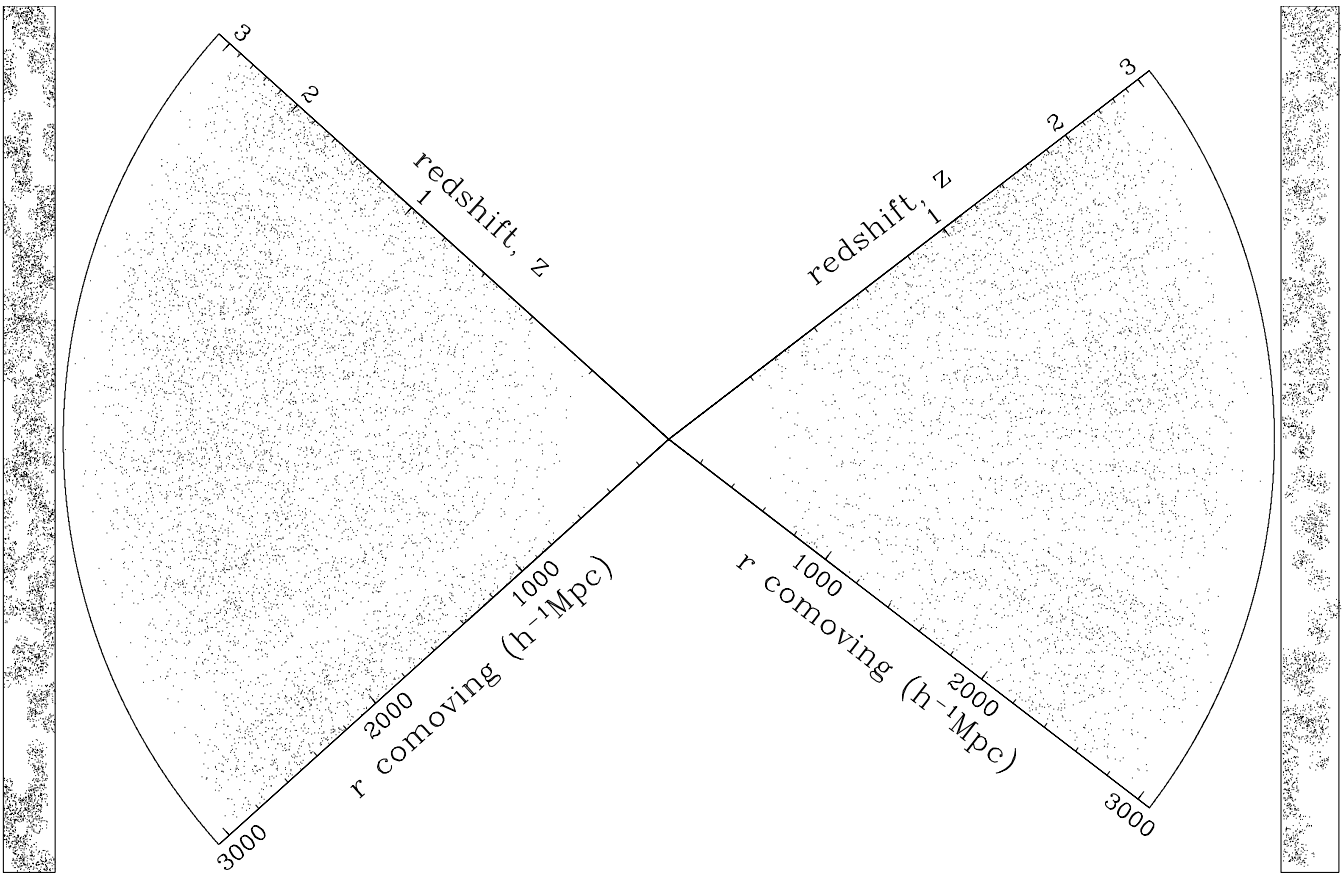

Figure 4. The distribution of 2QZ QSOs in the 10 k catalogue. Note that only objects at $0.3 < z \leq 2.9$ are used in our analysis. The SGC strip is on the left, the NGC on the right. The rectangular regions show the distribution projected on to the sky in each strip.

discussed in Section 2.2: (1) full accounting for non-uniform coverage; (2) taking only completely observed regions; and (3) using the QSO (α, δ) for the random point positions. These are presented in Figs 5(a), (b) and (c) respectively. The results demonstrate that QSO clustering follows a power law on small to intermediate scales. There is some evidence of a break in the power law at $\sim 35\,h^{-1}$ Mpc. We fit a power law of the conventional form,

$$\xi(s) = \left(\frac{s}{s_0}\right)^{-\gamma}. \tag{8}$$

The best fits using the maximum likelihood technique are $(s_0, \gamma) = (3.99^{+0.28}_{-0.34}, 1.58^{+0.10}_{-0.09})$, $(4.59^{+0.37}_{-0.39}, 1.64^{+0.12}_{-0.12})$ and $(3.87^{+0.29}_{-0.32}, 1.63^{+0.11}_{-0.11})$ for methods 1, 2 and 3 respectively, where s_0 is in units of h^{-1} Mpc. We fit the power law on scales 0.7–$35h^{-1}$ Mpc. The minimum scale is set by the smallest scale at which we find QSO pairs, and the maximum scale is set by the scale of the observed break in $\xi(s)$. A comparison of all three methods is shown in Fig. 5(d). Here we also plot separately the clustering of the NGC and SGC strips.

First, we note that the signals from the NGC and SGC strips are consistent. The NGC has no pairs at very small scales ($<1.5\,h^{-1}$ Mpc); however, the SGC strip contains only three pairs at these scales, and fewer are expected in the NGC owing to the smaller number of objects in this strip (4005 in the NGC versus 6553 in the SGC). Secondly, there appears to be no significant difference between our different estimations of $\xi_{\rm Q}$. Method 2 shows a slightly higher signal, while method 3 is marginally lower

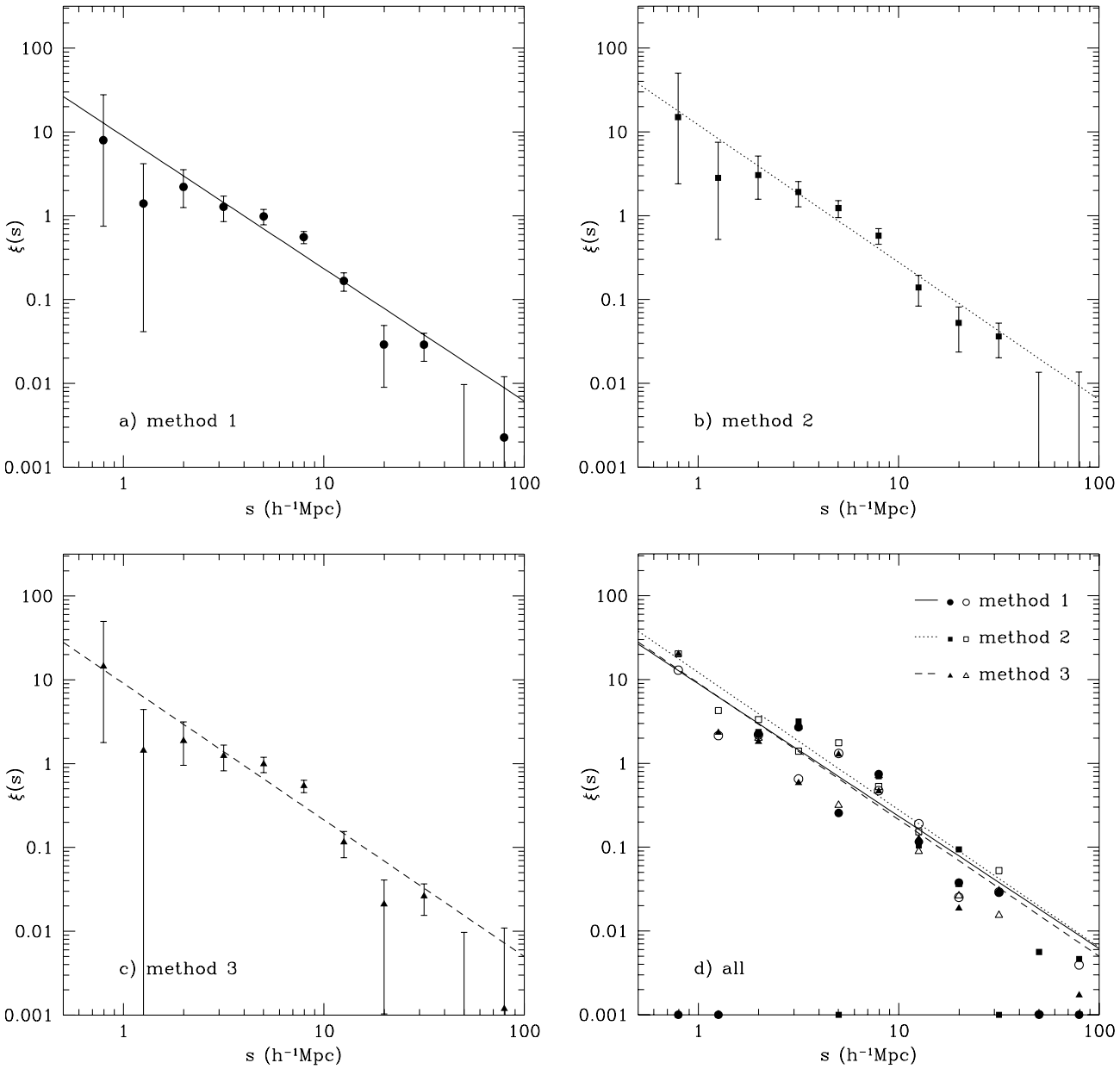

Figure 5. The two-point correlation function for 2QZ QSOs in the redshift interval $0.3 < z \leq 2.9$ for an EdS cosmology, using the different estimators discussed in the text: (a) method 1; (b) method 2; (c) method 3; and (d) all three methods. In plots (a), (b) and (c) we show $\xi_{\rm Q}$ from the combined NGC and SGC strips with the best-fitting power law at $s \leq 35h^{-1}$ Mpc in each case. In (d) we compare the three methods, the two points for each method being separate estimates in the NGC (filled symbols) and SGC (open symbols) strips. The lines are identical to those in (a), (b) and (c) denoting the best-fitting power law in each method.

than the other two methods. We estimate how much of the difference between methods 1 and 3 could be due to the removal of real signal by taking the measured correlation function from method 1 and integrating it over our redshift range, weighted by the QSO redshift distribution. This then gives us an angular correlation function with which we weight the random distribution when deriving the three-dimensional correlation, so suppressing the angular component. The results of this analysis are shown in Fig. 6. On small scales there is very little effect on the three-dimensional clustering; however, on scales $\gtrsim 20\,h^{-1}$ Mpc the clustering signal becomes suppressed by larger amounts (dotted line). The correlation functions measured from the data using the two methods are also plotted in Fig. 6. The difference in the measured values at $\gtrsim 20\,h^{-1}$ Mpc is similar to that predicted by the model, suggesting that some large-scale power is removed by method 3. We therefore choose to use method 1 throughout the remainder of our analysis (method 2 contains half as many QSOs as method 1, only 5348, and they are generally distributed in many small overlap regions, the dark shaded regions in Fig. 1). Any residual systematic errors caused by the variable observational completeness are not significant enough to affect any of the conclusions of this paper.

We also calculate ξ_Q for the Λ cosmology, with $\Omega_0 = 0.3$ and $\lambda_0 = 0.7$. This is compared with the method 1 estimate for the EdS case in Fig. 7. The effect of introducing a significant cosmological

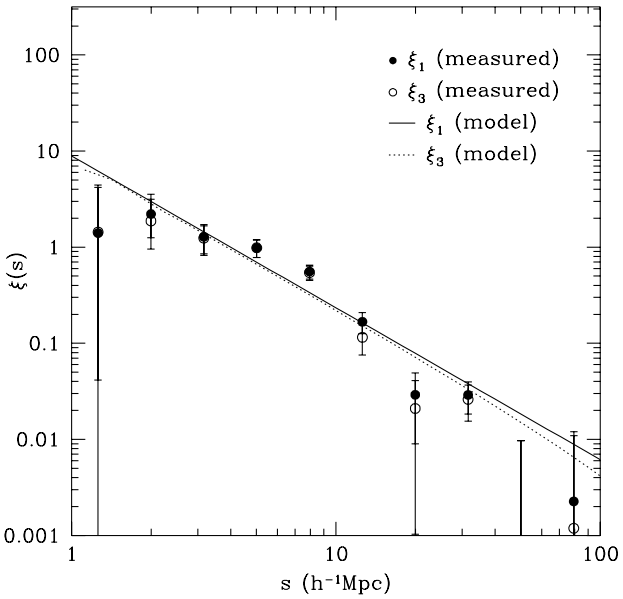

Figure 6. The estimated effect of using actual QSO (α, δ) for the random distribution when estimating the correlation function (method 3; dotted line). The solid line is the input model power-law (identical to the power-law fit to method 1). The filled and open circles are the estimates of ξ_Q from the data using methods 1 and 3 respectively.

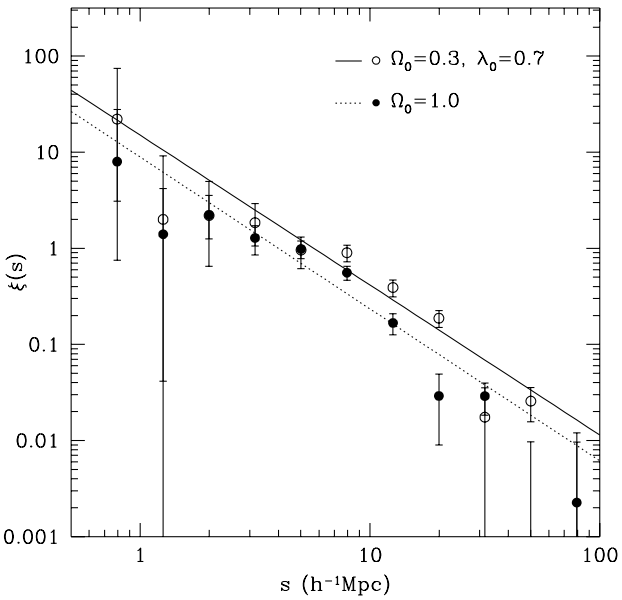

Figure 7. A comparison between the 2QZ $\xi_Q(s)$ for different cosmologies: EdS (filled circles) and Λ (open circles). The solid and dotted lines are the best-fitting power laws in each case.

Table 1. 2QZ clustering results for various cosmologies and redshift intervals. The s_0 and γ are best-fitting values. The results for the two-parameter fit are allowing both s_0 and γ to vary freely. For the one-parameter fit we constrain γ to be the best-fitting value for each cosmology over the full redshift interval ($0.30 < z \leq 2.90$), and allow only s_0 to vary. The value of the reduced χ^2 for each fit are also listed.

				two-parameter fit			one-parameter fit		
(Ω_0,λ_0)	redshift range	$\bar{z}$	N_Q	s_0	γ	χ^2	s_0	χ^2	$\bar{\xi}(20)$
(1.0,0.0)	$0.30 < z \leq 2.90$	1.49	10558	$3.99^{+0.28}_{-0.34}$	$1.58^{+0.10}_{-0.09}$	1.42	–	–	0.197 ± 0.026
(0.3,0.7)	$0.30 < z \leq 2.90$	1.49	10558	$5.69^{+0.42}_{-0.50}$	$1.56^{+0.10}_{-0.09}$	1.33	–	–	0.416 ± 0.048
(1.0,0.0)	$0.30 < z \leq 0.95$	0.69	2299	$3.84^{+0.56}_{-0.69}$	$1.70^{+0.27}_{-0.36}$	1.14	$3.65^{+0.56}_{-0.56}$	1.18	0.163 ± 0.054
(1.0,0.0)	$0.95 < z \leq 1.35$	1.16	2116	$2.72^{+0.94}_{-1.18}$	$1.25^{+0.27}_{-0.25}$	1.37	$3.55^{+0.61}_{-0.64}$	1.27	0.211 ± 0.057
(1.0,0.0)	$1.35 < z \leq 1.70$	1.53	2177	$3.49^{+0.61}_{-0.70}$	$1.63^{+0.22}_{-0.22}$	1.51	$3.41^{+0.56}_{-0.56}$	1.53	0.192 ± 0.052
(1.0,0.0)	$1.70 < z \leq 2.10$	1.89	2186	$4.31^{+0.55}_{-0.61}$	$1.83^{+0.21}_{-0.20}$	0.64	$3.85^{+0.56}_{-0.56}$	0.87	0.140 ± 0.055
(1.0,0.0)	$2.10 < z \leq 2.90$	2.36	1780	$4.43^{+0.77}_{-0.94}$	$1.84^{+0.30}_{-0.30}$	1.14	$3.96^{+0.80}_{-0.83}$	1.35	0.099 ± 0.078
(0.3,0.7)	$0.30 < z \leq 0.95$	0.69	2299	$5.28^{+0.72}_{-0.89}$	$1.72^{+0.23}_{-0.22}$	1.21	$4.90^{+0.71}_{-0.72}$	1.28	0.269 ± 0.085
(0.3,0.7)	$0.95 < z \leq 1.35$	1.16	2116	$4.05^{+1.21}_{-1.52}$	$1.38^{+0.27}_{-0.24}$	0.69	$4.65^{+0.89}_{-0.91}$	0.63	0.371 ± 0.102
(0.3,0.7)	$1.35 < z \leq 1.70$	1.53	2177	$5.23^{+0.92}_{-1.08}$	$1.55^{+0.21}_{-0.20}$	1.92	$5.24^{+0.82}_{-0.81}$	1.92	0.468 ± 0.103
(0.3,0.7)	$1.70 < z \leq 2.10$	1.89	2186	$6.24^{+0.86}_{-0.99}$	$1.80^{+0.21}_{-0.19}$	0.83	$5.54^{+0.84}_{-0.86}$	1.09	0.394 ± 0.110
(0.3,0.7)	$2.10 < z \leq 2.90$	2.36	1780	$6.93^{+1.32}_{-1.64}$	$1.64^{+0.29}_{-0.27}$	1.26	$6.68^{+1.23}_{-1.27}$	1.30	0.615 ± 0.178

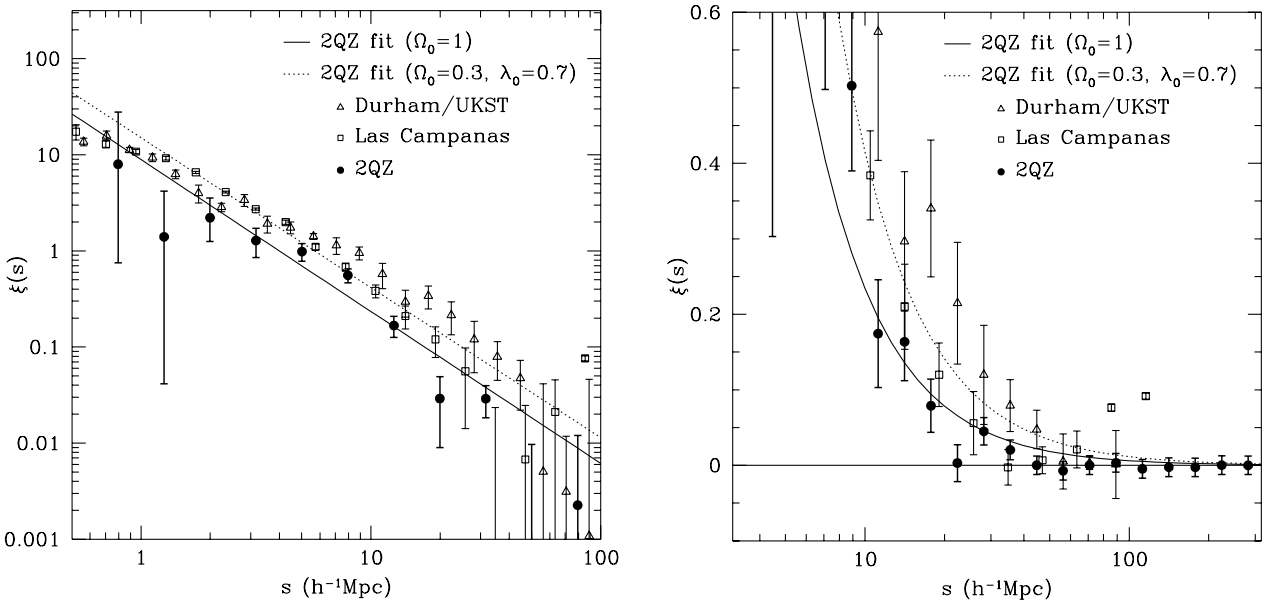

Figure 8. The two-point correlation function for 2QZ QSOs in the redshift interval $0.3 < z \leq 2.9$ in an EdS cosmology, compared with the clustering of local galaxies from the Durham/UKST Survey (Ratcliffe et al. 1998, triangles) and the Las Campanas Survey (Tucker et al. 1997, squares), plotted in (a) log–log space to highlight smaller scales, and (b) log–linear space to highlight larger scales. In (a) the 2QZ data are plotted in $\log(\Delta s) = 0.2$ bins, while in (b) $\log(\Delta s) = 0.1$. The solid line is the best-fitting power law to the 2QZ data for the EdS cosmology, while the dotted line is the best fit for the Λ cosmology. The 2QZ data points for the Λ model are omitted for clarity.

constant term is to increase the relative separation of QSOs, and hence increase the clustering scalelength. The break in the power law is now seen at $\simeq 60\,h^{-1}$ Mpc; we therefore make our power-law fits out to this scale. The best-fitting power law for the Λ cosmology is $(s_0, \gamma) = (5.69^{+0.42}_{-0.50}, 1.56^{+0.10}_{-0.09})$. All results are listed in Table 1.

3.2 QSO clustering compared with local galaxies

In Fig. 8 we compare our QSO clustering results at $\bar{z} = 1.49$ with galaxy clustering at low redshift ($z \sim 0.05$), in particular, the Las Campanas (Tucker et al. 1997) and Durham/UKST (Ratcliffe et al. 1998) galaxy surveys (open squares and triangles respectively). We see that there is good general agreement between the galaxy and QSO clustering, although the samples have differing redshift ranges. The EdS $\xi_{\rm Q}$ is slightly lower on average than $\xi_{\rm gal}$, while $\xi_{\rm Q}$ in the Λ cosmology is closer in amplitude to the galaxies. Both QSOs and galaxies show a break in $\xi(r)$ at $\sim 40\,h^{-1}$ Mpc. We note that the errors on $\xi_{\rm Q}$ are smaller than those on $\xi_{\rm gal}$ at $>20\,h^{-1}$ Mpc.

3.3 QSO clustering compared with CDM

In order to compare directly with theory, and include all non-linear effects and redshift-space distortions, we have used the *Hubble* Volume simulations of the Virgo Consortium (Colberg et al. 1998). We have produced mock 2QZ QSO catalogues with the same survey geometry and explicitly included evolution of the density field by outputting the simulation at different times along the light cone. A detailed discussion of the simulations, including a number of biasing models, will be given by Hoyle et al. (in preparation). Here we simply compare the dark matter correlation function averaged over the light cone with the 2QZ data. In particular we compare the redshift-space mass correlation function of a ΛCDM model with $\xi_{\rm Q}$. This model has $\Omega_0 = 0.3$, $\Omega_{\rm baryon} = 0.04$, $\lambda_0 = 0.7$, $\sigma_8 = 0.9$, $h = 0.7$ and an effective shape parameter,

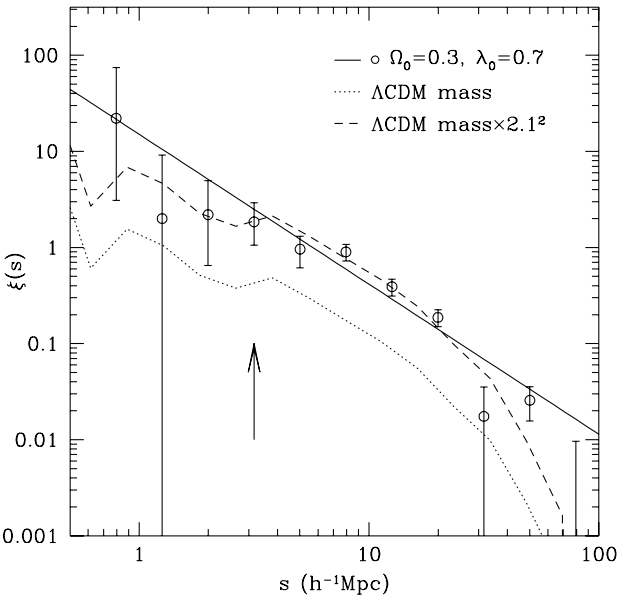

Figure 9. A comparison between the 2QZ $\xi_{\rm Q}$ (open circles) and ξ_ρ (dotted line) from the *Hubble* Volume simulations in the Λ cosmology. The dashed line is $2.1^2 \times \xi_\rho$. The arrow marks the resolution limit of the simulation. Also shown is the best-fitting power law (solid line).

taking into account the baryon component (Sugiyama 1995), of $\Gamma_{\rm eff} = 0.17$. The model and data are shown in Fig. 9. The amplitude of $\xi_{\rm Q}$ is $\sim$4 times larger than the ΛCDM mass correlation function, ξ_ρ. When scaled by this factor, the model and data appear to be well matched with a best-fitting bias value of 2.1.

Increasing the value of $\Gamma_{\rm eff}$ will move the models away from the data by steepening ξ_ρ at large scales. We do not have a large suite of simulations with which to compare the effect of changing $\Gamma_{\rm eff}$ and cosmology. However, on the scales that we are fitting, linear theory is a reasonable approximation. Therefore the effect of

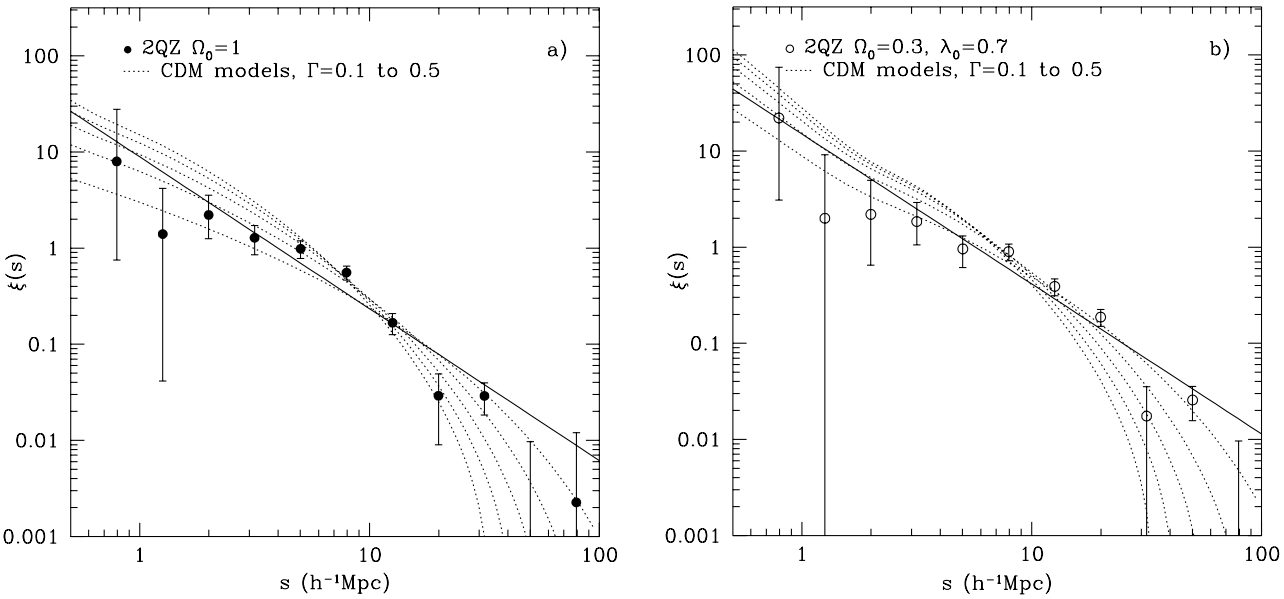

Figure 10. A comparison between the 2QZ $\xi_{\rm Q}$ and CDM-type models in the (a) EdS and (b) Λ cosmologies. The dotted lines are non-linear CDM correlation functions with various values of $\Gamma_{\rm eff}$ scaled by a linear bias to give the best fit to the 2QZ data. $\Gamma_{\rm eff} = 0.1$, 0.2, 0.3, 0.4 and 0.5 from top to bottom at large scales. The solid lines are the best-fitting power laws in each case.

redshift-space distortions will be simply to scale ξ by $(1 + 2\beta/3 + \beta^2/5)$ where $\beta \simeq \Omega_0^{0.6}/b$ (Kaiser 1987). We can then simply absorb this factor into an effective linear bias factor. We then fit model real space non-linear correlation functions at $z = 1.49$ to the data (again at scales 5 to $100\,h^{-1}$ Mpc) using the ansatz of Peacock & Dodds (1996) to determine the non-linear correction to the model ξ. The deviation from non-linearity is small (typically $\lesssim$5 per cent) on the scales of interest. We do not take into account small-scale non-linear velocity dispersions in our model; however, these should be small at the scales and redshifts considered. We also do not consider the effects of redshift measurement errors on $\xi(s)$; these again should only be a factor on small, $\lesssim 5\,h^{-1}$ Mpc, scales. We use five different models with $\Gamma_{\rm eff} = 0.1$, 0.2, 0.3, 0.4 and 0.5, and fit for the effective linear bias value. The results of this procedure are shown in Fig. 10. In the EdS cosmology, models with $\Gamma_{\rm eff} = 0.2$, 0.3 and 0.4 are acceptable at the 10 per cent level, while $\Gamma_{\rm eff} = 0.1$ and 0.5 are ruled out at greater than 90 per cent confidence. The main reason that a broad range of models are acceptable is the relatively low point at $\sim 20\,h^{-1}$ Mpc in $\xi_{\rm Q}$. In the Λ cosmology the $\Gamma_{\rm eff} = 0.1$ and 0.2 models are the only ones to agree with the data, the others being ruled out at greater than 99.9 per cent confidence. Thus the QSO correlation function detects excess large-scale power over what is expected in the $\Gamma_{\rm eff} = 0.5$ *standard* CDM model, confirming the results from the APM galaxy survey (Maddox et al. 1990).

The required $\Gamma_{\rm eff}$ is larger in the Λ cosmology, as structure is moved to larger scales. This suggests a test with the full 2QZ which will be devoid of observational incompleteness as well as having increased statistical accuracy. The break of the correlation function in a CDM-type cosmology can be used as a standard rod to determine cosmological parameters, in particular λ_0, if it is at linear scales. For example, if at low redshift the shape is well defined, then if the break is in the linear theory regime it should remain at the same scale at high redshift. Measuring the break at a different scale at high redshift would imply that the wrong cosmological parameters were being used in the determination of the high-redshift correlation function. This is similar to the geometric tests discussed by several authors (Alcock & Paczynski 1979; Phillipps 1994; Ballinger, Peacock & Heavens 1996), but has the advantage of not being affected by redshift-space distortions if clustering can be measured on a sufficiently large scale. This is because linear redshift-space distortions affect only the amplitude and not the shape of ξ. Shanks & Boyle (1994) proposed a similar method, using linear features in the correlation function on $\gtrsim 100\,h^{-1}$ Mpc scales.

4 EVOLUTION OF QSO CLUSTERING

4.1 Measurements of QSO clustering evolution

In the previous section we calculated $\xi_{\rm Q}$ averaged over a large redshift interval. We now split the 2QZ QSO sample up into five redshift intervals containing approximately equal numbers of QSOs. The exact limits and numbers of QSOs are given in Table 1. The measured $\xi_{\rm Q}(s)$ are shown in Fig. 11 for the EdS cosmology. QSO clustering appears to vary little over the entire redshift range that we consider. The data points are consistent with the redshift-averaged $\xi_{\rm Q}$ (dotted line in Fig. 11). For each redshift interval we fit a power law, the results of which are shown in Table 1 and by the solid lines in Fig. 11. As for the redshift-averaged analysis, we fit the power law within $35\,h^{-1}$ Mpc. We similarly fit $\xi_{\rm Q}$ in redshift intervals for the Λ cosmology (Fig. 12) using the $60\,h^{-1}$ Mpc maximum as above. Again there is very little evidence of evolution. We note that there is some variation in the slope and amplitude of these power laws, but this appears to be mainly driven by the relatively low signal-to-noise ratio in each redshift bin. Great care should be taken when trying to interpret these power-law fit results, as amplitude and slope are correlated.

An alternative method to derive a measurement of evolution is to constrain the power-law slope and fit only for the scalelength, s_0. This should be valid as we do not see any evidence for significant evolution in the slope of $\xi_{\rm Q}$. We constrain the slope to be that found over the full redshift range (Section 3), $\gamma = 1.58$ for the EdS cosmology and $\gamma = 1.56$ for the Λ cosmology. The results of this fitting process are seen in Table 1 and plotted in Fig. 13. In Table 1

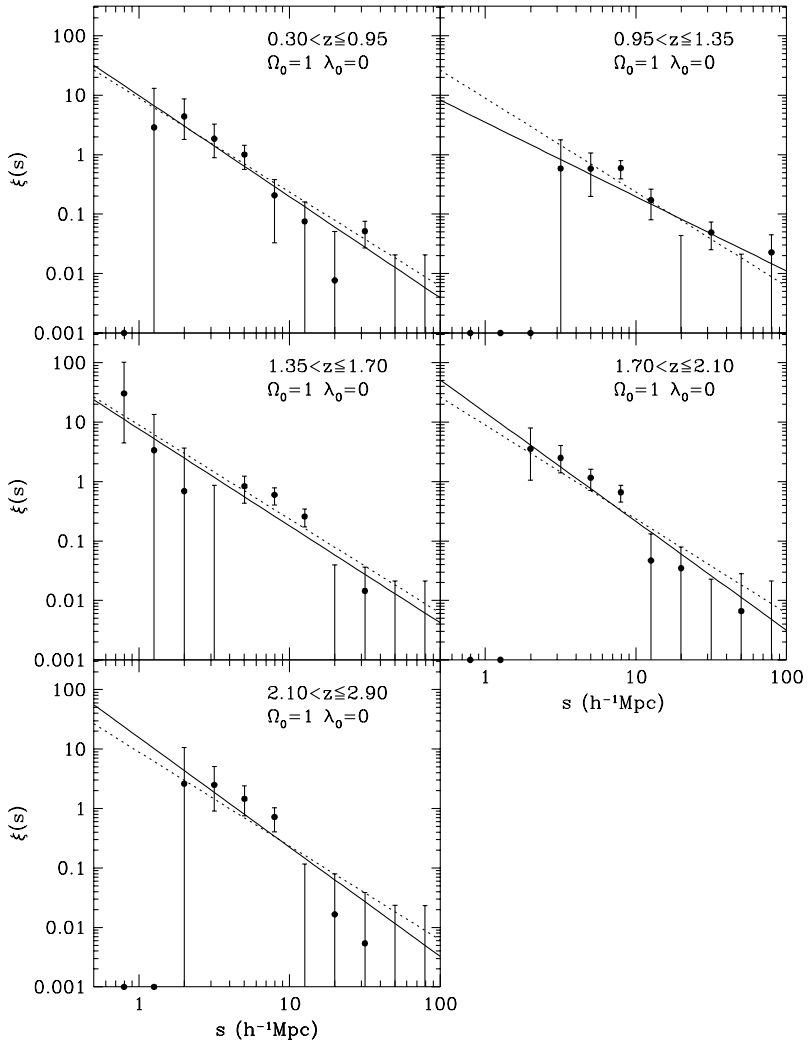

Figure 11. The two-point correlation function for 2QZ QSOs as a function of redshift for the EdS cosmology. Redshift increases, left to right and top to bottom. In each plot the solid line is the best-fitting power law on scales $\leq 35\,h^{-1}$ Mpc. The dotted line is the best fit to all the QSOs in the redshift range $0.3 < z \leq 2.9$ and is shown to aid comparison between redshift intervals. The points without error bars at $\xi(s) = 0.001$ are where there are zero QSO pair counts in a bin. These points are fully taken into account in the fitting process.

we also list the reduced χ^2 values for these fits. Limiting the fit to one parameter does not significantly alter the χ^2 values, demonstrating that the redshift-averaged power-law slope is a reasonable description of the data at all redshifts. Fig. 13(a) shows that in the EdS cosmology clustering is constant as a function of redshift. The Λ cosmology result is shown in Fig. 13(b). In this case there appears to be a marginal increase by a factor of $\sim$1.4 from $z = 0.7$ to 2.4. We compare our results in the EdS cosmology with previous QSO clustering results from CS96 and LAC98, using their measurements of $\bar{\xi}$ from 10 and $15\,h^{-1}$ Mpc to obtain a value of s_0 assuming a $\gamma = 1.58$ power law (the best-fitting power-law slope). Our results are in disagreement with those of LAC98, who find a $\sim 2\sigma$ increase in clustering between $z = 0.95$ and 1.8. A possible cause of this is cosmic variance, as LAC98 carry out their analysis in a single 24.6-deg^2 area of sky. However, given the large errors on the LAC98 data points, they only disagree with the 2QZ results at $\sim 2\sigma$ at $z = 1.8$.

A non-evolving clustering distribution has strong implications for models of structure and QSO formation. We first compare the 2QZ data with the simplest possible model, that of linear theory gravitational evolution in an $\Omega_0 = 1$ universe. This model is applicable when QSOs either directly trace the mass distribution, or have a bias that is constant as a function of redshift. When fitting linear theory to the evolution in s_0 for the EdS cosmology, we find that the model is rejected by the 2QZ data at 99.8 per cent confidence. In the Λ cosmology the linear theory evolution rate is reduced. However, in Fig. 13(b) we see that s_0 increases with redshift, although the significance of the increase is marginal: a constant s_0 as a function of redshift is not rejected by the data. When we try to fit linear evolution in this case it is rejected at >99.9 per cent significance. If we require that the normalization of the mass clustering be fixed by either the local abundance of massive clusters (Eke, Cole & Frenk 1996) or the four-yr *COBE* results (Bennett et al. 1996) then the mass clustering scalelength is forced to be less than $s_0(z = 0) \sim 5h^{-1}$ Mpc. In this case linear theory evolution is even more clearly rejected by the 2QZ data. It therefore appears that QSO clustering cannot follow the linear evolution of the density field, and QSO bias must be a function of redshift.

We should also make comparisons with galaxy clustering measurements. The typical scalelength found in local galaxy surveys is $s_0 \sim 5$–$6h^{-1}$ Mpc, only marginally higher than the 2QZ

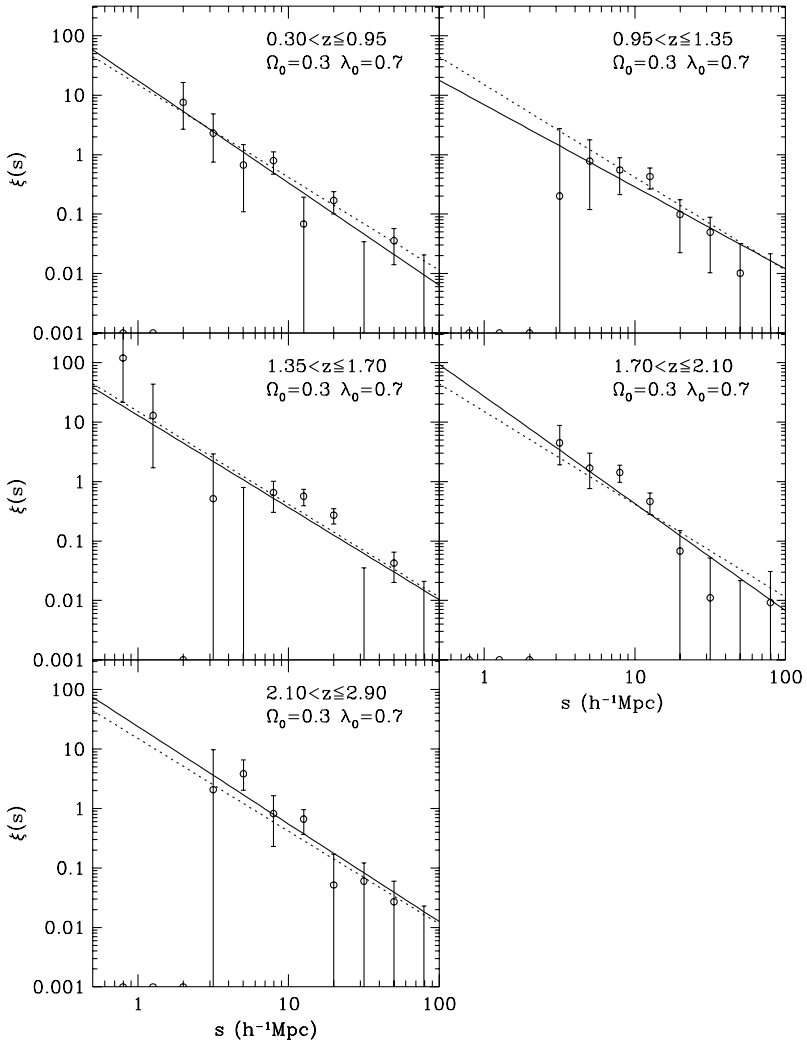

Figure 12. The two-point correlation function for 2QZ QSOs as a function of redshift for the Λ cosmology. Redshift increases, left to right and top to bottom. In each plot the solid line is the best-fitting power law on scales $\leq 60\,h^{-1}$ Mpc. The dotted line is the best fit to all the QSOs in the redshift range $0.3 < z \leq 2.9$ and is shown to aid comparison between redshift intervals.

results for the EdS cosmology, and identical to the values found in the Λ cosmology. At $z \sim 3$ Adelberger et al. (1998) find a scalelength of $r_0 \sim 4$–$6h^{-1}$ Mpc for Lyman-break galaxies, depending on the assumed cosmology. This again is very similar to the results derived from the 2QZ.

4.2 Comparison with biased models of clustering evolution

In the previous section we showed that for viable cosmological models, with evolution based on the gravitational growth of structure, QSOs do not simply trace the density fluctuations in the universe. Therefore QSOs are related to the mass distribution via a redshift-dependent bias. The form of this bias depends on the physical mechanisms of QSO formation.

The question of QSO lifetimes can be linked to their clustering. If QSOs have lifetimes that are cosmologically long (~a Hubble time), this would imply that QSOs are intrinsically rare. They could therefore be highly clustered, existing in rare high peaks in the density field (Efstathiou & Rees 1988), assuming that halo mass is the dominant factor in QSO formation. However, QSOs could form in a 'random' subset of less biased haloes, with the formation being driven by mechanisms other than mass, e.g. angular momentum.

Alternatively, QSOs could have shorter lifetimes, of the order of $\sim 10^6$–10^8 yr. There is mounting evidence for this, with the suggestion that most nearby galaxies appear to contain central supermassive black holes (e.g. Magorrian et al. 1998), so that most galaxies pass through a QSO/active galactive necleus (AGN) phase. They could therefore be clustered in a similar manner to galaxies. However, even if all galaxies go through a QSO/AGN phase, it is possible that this phase picks out a particular time in the evolution of galaxies, e.g. epochs of major star formation or merging. QSO clustering evolution can potentially help us to distinguish between a number of possible QSO formation mechanisms. However, we should be wary of over-interpreting models that do not include the uncertain physical mechanisms required for QSO formation.

4.2.1 A long-lived QSO model

The next simplest assumption, after assuming that bias does not evolve with redshift, is that QSOs are long-lived (with ages of the

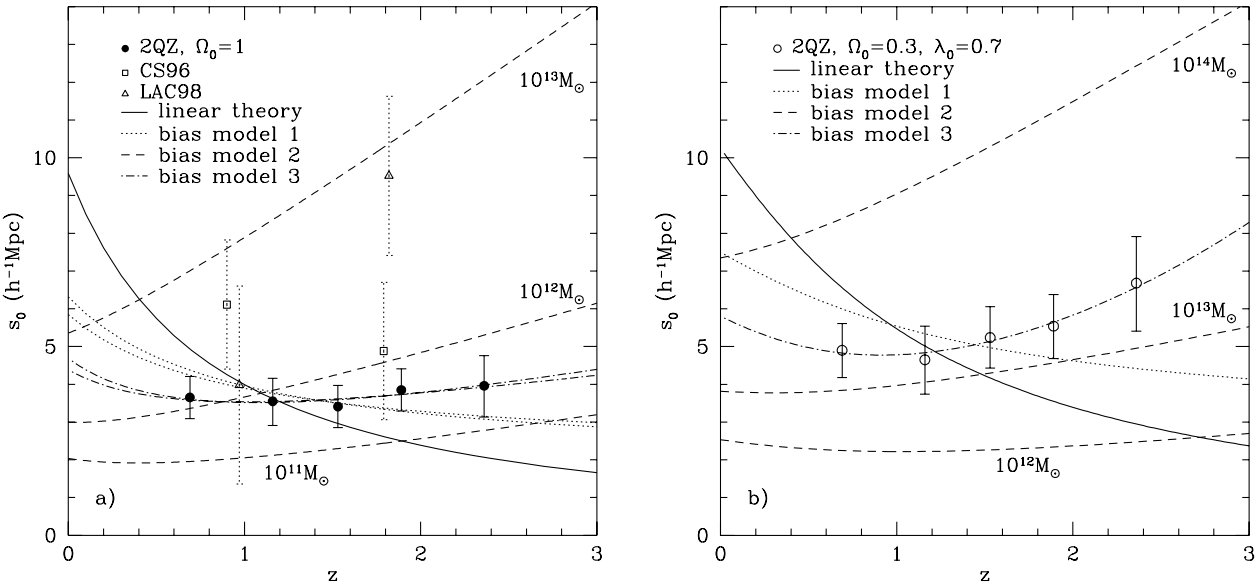

Figure 13. The best-fitting values for s_0 with fixed γ as a function of redshift in the (a) EdS and (b) Λ cosmologies. The solid lines show the best-fitting linear theory evolution model in each case. The dotted lines show the best-fitting long-lived QSO biasing model (bias model 1) from Section 4.2.1. The dashed lines show the models of Matarrese et al. (1997) (bias model 2) for different values of the minimum halo mass. The dot–dashed lines show the best-fitting empirical bias model (bias model 3). In (a) the two dotted and dot–dashed lines are for *COBE* (top at $z = 0$) and cluster (bottom at $z = 0$) normalization.

order of a Hubble time). We assume that, after formation at some arbitrarily high redshift, the subsequent evolution of QSO clustering is governed purely by their motion within the gravitational potential produced by the density fluctuations in the Universe (Fry 1996). This then implies a bias which evolves as

$$b(z) = 1 + [b(0) - 1]G(\Omega_0, \lambda_0, z). \quad (9)$$

We call this bias model 1. $G(\Omega_0, \lambda_0, z)$ is the linear growth rate of density perturbations, which for an EdS cosmology is $1 + z$. For the cosmological dependence of the growth rate we use the accurate fitting formula of Carroll, Press & Turner (1992), which is good to a few per cent [note that our $G(\Omega_0, \lambda_0, z)$ is the full evolution term, and should not be confused with the function of Carroll et al. which contains only the cosmological dependence]. The biasing model of equation (9) is also equivalent to QSOs forming in peaks of the density field above a constant threshold (CS96). This model places certain limitations on the form of evolution. First, bias will tend to unity as time increases. Secondly, positive evolution (an increase in clustering) as redshift increases is not possible. This is because at most the bias evolves only as fast as $G(\Omega_0, \lambda_0, z)$, cancelling out the growth in the density field.

For comparison with the observed clustering, we have normalized the mass evolution in two ways: using both local cluster abundances (Eke et al. 1996) and the 4-yr *COBE* results (Bennett et al. 1996). We calculate $s_0(z)$ for the mass assuming a CDM power spectrum with a shape parameter of $\Gamma_{\rm eff} = 0.25$ (varying the shape parameter $\Gamma_{\rm eff}$ only has an impact on the normalization when using the *COBE* data). In the EdS cosmology the s_0 fits give $b(0) = 1.82^{+0.07}_{-0.07}$ $(1.62^{+0.07}_{-0.06})$ for cluster (*COBE*) normalization. These correspond to $\sigma_8 \simeq 1$ for QSOs at $z = 0$ (σ_8 for mass fluctuations is 0.52 and 0.65 for cluster and *COBE* normalization respectively), which is the same as the nominal $\sigma_8 \sim 1$ value found for local galaxies.

Schade, Boyle & Letawsky (2000) find that at low redshift typical QSOs and AGN (where by typical we mean at or around the break in the luminosity function) have host galaxies that are remarkably similar to normal galaxies, except for a bias towards spheroid-dominated galaxies. Approximately 55 per cent of their sample have hosts that are best fitted by a bulge-only model. Elliptical galaxies are well known to be more strongly clustered than spirals (Loveday et al. 1995), with a relative bias factor of $b_{\rm e,s} \simeq 1.9$. Correcting for this morphological segregation gives an expected $\sigma_8 = 1.2$–1.3 for QSOs at low redshift, approximately in line with the above value.

For the Λ cosmology a biased model of the form in equation (9) provides only a marginally adequate fit to the data (rejected at 88 per cent) with a best-fitting bias of $b(0) = 1.84^{+0.08}_{-0.08}$. This is because the model cannot reproduce the increase in clustering strength at high redshift visible in this cosmology. The hypothesis that QSOs have cosmologically long (∼Hubble time) lifetimes therefore appears unlikely in the Λ cosmology.

4.2.2 *More general models of biasing*

The above simple model of biasing can be extended in a number of ways. The most obvious is to remove the constraint that objects formed at an arbitrarily high redshift, and allow objects to continue to form at lower redshift. The problem then becomes one of deciding how and when objects do form. A natural method for deciding when dark matter haloes form is based on an application of the Press–Schechter (1974) formalism which describes the evolution of the number density of dark matter haloes. Working within this formalism, Mo & White (1996) have obtained an approximation for the linear bias of dark matter haloes as a function of mass. Matarrese et al. (1997) have used these ideas to provide biasing models in a *COBE*-normalized $\Omega_0 = 1$ universe assuming a CDM power spectrum with a shape parameter of $\Gamma_{\rm eff} = 0.25$. These were extended to a number of different cosmological models by Moscardini et al. (1998). In particular, we are interested in the transient model of Matarrese et al., so called because the model does not require a normalization at $z = 0$. In this model, one assumes that all objects exceeding a given mass cut-off can be observed at any given redshift. The bias (which we call

model 2) then has the form

$$b(z) = 1 - 1/\delta_c + [b(0) - (1 - 1/\delta_c)]G(\Omega_0, \lambda_0, z)^{\beta}, \quad (10)$$

where δ_c is the critical linear overdensity for spherical collapse. For an EdS cosmology $\delta_c = 1.686$ for all redshifts; however, it varies away from this value by only a few per cent for the other cosmologies considered here (Lilje 1992). Matarrese et al. find the values of $b(0)$ and β by fitting to their Press–Schechter based models. These parameters depend on the minimum halo mass $M_{\rm min}$ considered. We compare this model of biasing to QSO clustering in an EdS universe in Fig. 13(a) for minimum halo masses of $M_{\rm min} = 10^{11}$, 10^{12} and $10^{13}\,{\rm M}_{\odot}$. In this cosmology the data are approximately consistent with a minimum halo mass of $10^{12}\,{\rm M}_{\odot}$ (although the model is still too steep), while the normalization is too low (*COBE* normalization) for lower mass haloes, and the evolution is too steep for higher mass haloes. In the Λ cosmology, we compare the *COBE*-normalized ΛCDM model of Moscardini et al.with our data. We note that this model is, in fact, for $\Omega_0 = 0.4$, $\lambda_0 = 0.6$. However, given the model and data uncertainties, these are adequate to make a general comparison with the 2QZ clustering evolution in the Λ cosmology. In this case we find that the data are more consistent with (although slightly above) a model with $M_{\rm min} \simeq 10^{13}\,{\rm M}_{\odot}$.

Although these models appear to describe the clustering evolution of QSOs adequately, it is not at all clear what the physical justification for this is. The models of Matarrese et al. assume that at each redshift QSOs inhabit the same mass haloes; this need not necessarily be the case. For example, Percival & Miller (1999) compare the evolution of bright QSOs, $-25.4 > M_B > -27.9$, with the dark matter halo formation rate in a number of cosmologies. They find that for an EdS universe, with a CDM-type power spectrum of shape parameter $\Gamma_{\rm eff} = 0.25$ which is cluster abundance normalized, the evolution of bright QSOs is best fitted by haloes of mass $\sim 10^{10.6}\,{\rm M}_{\odot}$. Our Λ cosmology increases the mass to $\sim 10^{11.8}\,{\rm M}_{\odot}$. These masses are $\sim 10\times$ smaller than those required to fit the 2QZ QSO clustering according to the models of Matarrese et al. This serves to demonstrate that we should be wary of over-interpreting fits to models that do not contain a physical description of QSO formation. For example, it is possible that QSO clustering is a function of luminosity, a point which has not been discussed in this paper, but will be investigated in future work.

4.2.3 *An empirical biasing description*

Lastly we fit a purely empirical biasing model to the data. For this model we use a generalization of equations (9) and (10) which is

$$b(z) = 1 + [b(0) - 1]G(\Omega_0, \lambda_0, z)^{\beta}, \quad (11)$$

where $b(0)$ and β are left free to be determined by fitting to the data. We call this form of bias evolution model 3. The normalization of the mass density field is set by either cluster or *COBE* normalization as in model 1. The dot–dashed lines in Fig. 13 show the best-fitting empirical model for each of our assumed cosmologies. In the EdS case we find $b(0) = 1.45^{+0.21}_{-0.16}$ and $\beta = 1.68^{+0.44}_{-0.40}$ [$b(0) = 1.28^{+0.16}_{-0.11}$ and $\beta = 1.89^{+0.49}_{-0.46}$] for cluster (*COBE*) normalization. As we might expect, the Λ cosmology has a larger β with the best-fitting parameters being $b(0) = 1.20^{+0.06}_{-0.02}$ and $\beta = 2.75^{+0.65}_{-0.57}$. The relatively high normalization in this cosmology and the low rate of mass clustering evolution mean that a large value of β is required to fit the data.

5 CONCLUSIONS

The preliminary release data set of the 2QZ contains 10 681 QSOs. It is already a factor of $\sim$25 larger than previous QSO surveys to this depth ($b_{\rm J} \leq 20.85$). When completed, the full sample will contain $\sim$25 000 QSOs. The current data set already allows us to measure the clustering of QSOs to unprecedented accuracy. In particular, we can summarize our work as follows:

(1) QSO clustering integrated over the redshift interval $0.3 < z \leq 2.9$ is well fitted by a power law on scales $\sim$1–35h^{-1} Mpc. In an Einstein–de Sitter universe the best-fitting power law has $s_0 = 3.99^{+0.28}_{-0.34}h^{-1}$ Mpc and $\gamma = 1.58^{+0.10}_{-0.09}$. Introducing a cosmological constant increases the distances between QSOs, so that the scalelength of clustering increases also. The power law then extends to $\sim 60\,h^{-1}$ Mpc and is best fitted by $s_0 = 5.69^{+0.42}_{-0.50}h^{-1}$ Mpc and $\gamma = 1.56^{+0.10}_{-0.09}$. These results are remarkably similar to the clustering of normal galaxies locally ($z \simeq 0.05$).

(2) We compare the clustering of 2QZ QSOs with the ΛCDM model and find that the shapes of model and data are consistent. A comparison with a family of CDM models with different shape parameters, $\Gamma_{\rm eff}$, finds that $\Gamma_{\rm eff} = 0.2$ to 0.4 provides an acceptable fit in the EdS cosmology. In the Λ cosmology only $\Gamma_{\rm eff} = 0.1$ or 0.2 provides an acceptable fit because of the movement of structure to larger scales. This suggests a test for cosmological parameters using the linear break in the correlation function which will be possible using the completed 2QZ data set.

(3) We measure the clustering amplitude of QSOs as a function of redshift, parametrized by s_0 assuming a fixed power-law slope. In an Einstein–de Sitter universe we find that QSO clustering is constant in comoving coordinates over the entire redshift range that we probe. In a Λ-dominated universe we find that clustering appears to increase (although constant clustering is not excluded) with increasing redshift. For both EdS and Λ cosmologies a model in which QSOs follow the same evolution as linear theory gravitational clustering (or have a bias that is constant as a function of redshift) is rejected at the >99 per cent level. If the constant clustering is extrapolated to $z \simeq 3$ it comfortably overlaps the clustering amplitude found for Lyman-break galaxies (Adelberger et al. 1998).

(4) We compare simple redshift-dependent bias models with the measured clustering evolution. We first use a model in which QSOs are long-lived (on cosmological time-scales), so that their clustering simply evolves according to their motion in the gravitational potential. This is consistent with 2QZ clustering evolution in an EdS case, and predicts $\sigma_8(z = 0) \simeq 1$ for QSOs, which is consistent with galaxy clustering. The long-lived model is not able to reproduce the increase in clustering seen in the Λ cosmology, and is marginally rejected at 88 per cent confidence. More complex models of QSO bias based on the Press–Schechter formalism have been developed by a number of authors. We use the models of Matarrese et al. (1997) and Moscardini et al. (1998) to make comparisons with the evolution of the 2QZ data set. These models adequately describe the 2QZ clustering evolution when the minimum halo mass considered is $M_{\rm min} \sim 10^{12}\,{\rm M}_{\odot}$ (EdS) or $M_{\rm min} \sim 10^{13}\,{\rm M}_{\odot}$ (Λ). However, without a convincing model of QSO formation, the interpretation of the comparison with these models of clustering evolution is questionable. We lastly derive a fit to an empirical biasing model based on power-law evolution of bias.

The large volumes sampled by QSO surveys allow structure to be investigated on the scales where growth is governed by linear

theory. Thus meaningful measurements of large-scale structure, which are easily related to the underlying cosmology, can be made irrespective of the relative bias of QSOs. QSOs therefore play an crucial role in linking low-redshift/small-scale galaxy clustering measurements to the fluctuations in the density field at high redshift seen in the cosmic microwave background. The completed 2QZ survey, without the current varying observational coverage, will allow detailed measurements of structure on a range of scales from $\sim$1 to 1000h^{-1} Mpc.

ACKNOWLEDGMENTS

This paper was prepared using facilities of the Anglo-Australian Observatory and the Starlink node at the Imperial College of Science, Technology and Medicine. The 2QZ is based on observations made with the Anglo-Australian Telescope and the UK Schmidt Telescope. NSL and FH are supported by PPARC studentships.

REFERENCES

Adelberger K. L., Steidel C. C., Giavalisco M., Dickinson M., Pettini M., Kellogg M., 1998, ApJ, 505, 18
Alcock C., Paczynski B., 1979, Nat, 281, 358
Andreani P., Cristiani S., 1992, ApJ, 398, L13
Bailey J., Glazebrook K., 1999, 2dF User Manual. Anglo-Australian Observatory
Ballinger W. E., Peacock J. A., Heavens A. F., 1996, MNRAS, 282, 877
Bennett C. L. et al., 1996, ApJ, 464, L1
Boyle B. J., Fong R., Shanks T., Peterson B. A., 1990, MNRAS, 243, 1
Boyle B. J., Shanks T., Croom S. M., 1995, MNRAS, 276, 33
Boyle B. J., Shanks T., Croom S. M., Smith R. J., Miller L., Loaring N., Heymans C., 2000, MNRAS, 317, 1014
Carlberg R. G. et al., 1999, Phil. Trans. R. Soc., 357, 167
Carroll S. M., Press W. H., Turner E. L., 1992, ARA&A, 30, 499
Colberg J. M. et al., 1998, in Colombi S., Meller Y., Rabin B., eds, 14th IAP meeting, Wide Field Surveys in Cosmology. Editions Frontières, Paris, p. 247
Colless M. et al., 1999, in Morganti R., Couch W. J., eds, Proc. ESO/Australia Workshop, Looking Deep in the Southern Sky. Springer-Verlag, Berlin, p. 9
Croom S. M., 1997, PhD thesis, Univ. Durham
Croom S. M., Shanks T., 1996, MNRAS, 281, 893 (CS96)
Croom S. M., Ratcliffe A., Parker Q. A., Shanks T., Boyle B. J., Smith R. J., 1999, MNRAS, 306, 592
Croom et al., 2001, MNRAS, 322, L29
Efstathiou G., Rees M. J., 1988, MNRAS, 230, 5P
Eke V. R., Cole S., Frenk C. S., 1996, MNRAS, 282, 263
Fry N. J., 1996, ApJ, 461, L65
Gehrels N., 1986, ApJ, 303, 336
Iovino A., Shaver P. A., 1988, ApJ, 330, L13
Kaiser N., 1987, MNRAS, 227, 1
La Franca F., Andreani P., Cristiani S., 1998, ApJ, 497, 529 (LAC98)
Landy S. D., Szalay A. S., 1993, ApJ, 412, 64
Le Fevre O., Hudon D., Lilly S. J., Crampton D., Hammer F., Tresse L., 1996, ApJ, 461, 534
Lilje P. B., 1992, ApJ, 386, L33
Loveday J., Maddox S. J., Efstathiou G., Peterson B. A., 1995, ApJ, 442, 457
Maddox S. J., Efstathiou G., Sutherland W. J., Loveday J., 1990, MNRAS, 242, 43P
Magorrian J. et al., 1998, AJ, 115, 2285
Mann R. G., Peacock J. A., Heavens A. F., 1998, MNRAS, 293, 209
Matarrese S., Coles P., Lucchin F., Moscardini L., 1997, MNRAS, 286, 115
Mo H. J., Fang L. Z., 1993, ApJ, 410, 493
Mo H. J., White S. D. M., 1996, MNRAS, 282, 347
Mo H. J., Jing Y. P., Borner G., 1992, ApJ, 392, 452
Moscardini L., Coles P., Lucchin F., Matarrese S., 1998, MNRAS, 299, 95
Osmer P. S., 1981, ApJ, 247, 762
Peacock J. A., 1997, MNRAS, 284, 885
Peacock J. A., Dodds S. J., 1996, MNRAS, 280, L19
Pervical W., Miller L., 1999, MNRAS, 309, 823
Phillipps S., 1994, MNRAS, 269, 1007
Postman M., Lauer T. R., Szapudi I., Oegerle W., 1998, ApJ, 506, 33
Press W. H., Schechter P., 1974, ApJ, 187, 425
Ratcliffe A., Shanks T., Parker Q. A., Fong R., 1998, MNRAS, 296, 173
Schade D., Boyle B. J., Letawsky M., 2000, MNRAS, 315, 498
Schlegel D. J., Finkbeiner D. P., Davis M., 1998, ApJ, 500, 525
Shanks T., Boyle B. J., 1994, MNRAS, 271, 753
Shanks T., Fong R., Boyle B. J., Peterson B. A., 1987, MNRAS, 227, 739
Shaver P. A., 1984, A&A, 136, L9
Smith R. J., 1998, PhD thesis, Univ. Cambridge
Smith R. J., Croom S. M., Boyle B. J., Shanks T., Miller L., Loaring N. A., 2001, MNRAS, submitted
Steidel C. C., Adelberger K. L., Dickinson M., Giavalisco M., Pettini M., Kellogg M., 1998, ApJ, 492, 428
Sugiyama N., 1995, ApJS, 100, 281
Taylor K., Cannon R. D., Watson F. G., 1997, in Ardeberg A. L., ed., Proc. SPIE Conf. 2871, Optical Telescopes of Today and Tomorrow. SPIE, Bellingham, p. 145
Tucker D. L. et al., 1997, MNRAS, 285, L5
Weinberg S., 1972, Gravitation and Cosmology. Wiley, New York

This paper has been typeset from a TEX/LATEX file prepared by the author.